JACS
JOURNAL OF THE AMERICAN CHEMICAL SOCIETY
Article
pubs.acs.org/JACS

Interplay of Experiment and Theory in Elucidating Mechanisms of Oxidation Reactions by a Nonheme $Ru^{IV}O$ Complex

Sunder N. Dhuri,[†,‡,∥] Kyung-Bin Cho,[†,∥] Yong-Min Lee,[†] Sun Young Shin,[†] Jin Hwa Kim,[†] Debasish Mandal,[§] Sason Shaik,[§] and Wonwoo Nam*[,†]

[†]Department of Chemistry and Nano Science, Ewha Womans University, Seoul 120-750, Korea

[‡]Department of Chemistry, Goa University, Goa 403 206, India

[§]Institute of Chemistry and the Lise Meitner-Minerva Center for Computational Quantum Chemistry, The Hebrew University of Jerusalem, 91904 Jerusalem, Israel

Supporting Information

ABSTRACT: A comprehensive experimental and theoretical study of the reactivity patterns and reaction mechanisms in alkane hydroxylation, olefin epoxidation, cyclohexene oxidation, and sulfoxidation reactions by a mononuclear nonheme ruthenium(IV)−oxo complex, $[Ru^{IV}(O)(terpy)(bpm)]^{2+}$ (**1**), has been conducted. In alkane hydroxylation (i.e., oxygen rebound vs oxygen non-rebound mechanisms), both the experimental and theoretical results show that the substrate radical formed via a rate-determining H atom abstraction of alkanes by **1** prefers dissociation over oxygen rebound and desaturation processes. In the oxidation of olefins by **1**, the observations of a kinetic isotope effect (KIE) value of 1 and styrene oxide formation lead us to conclude that an epoxidation reaction via oxygen atom transfer (OAT) from the $Ru^{IV}O$ complex to the C=C double bond is the dominant pathway. Density functional theory (DFT) calculations show that the epoxidation reaction is a two-step, two-spin-state process. In contrast, the oxidation of cyclohexene by **1** affords products derived from allylic C−H bond oxidation, with a high KIE value of 38(3). The preference for H atom abstraction over C=C double bond epoxidation in the oxidation of cyclohexene by **1** is elucidated by DFT calculations, which show that the energy barrier for C−H activation is 4.5 kcal mol^{-1} lower than the energy barrier for epoxidation. In the oxidation of sulfides, sulfoxidation by the electrophilic Ru−oxo group of **1** occurs via a direct OAT mechanism, and DFT calculations show that this is a two-spin-state reaction in which the transition state is the lowest in the $S = 0$ state.

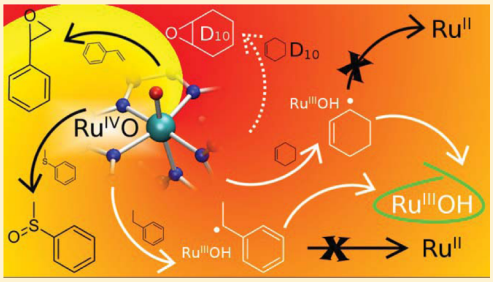

INTRODUCTION

High-valent metal−oxo complexes of heme and nonheme ligands perform a wide range of biological oxidation reactions, such as alkane hydroxylation, olefin epoxidation, and sulfoxidation.[1−10] The reactivities and reaction mechanisms of the metal−oxo complexes have been investigated intensively over the past several decades because of their tremendous potential for industrial and biomimetic uses. For example, a large number of high-valent $Fe^{IV}O$ complexes have been synthesized and investigated in heme and nonheme systems, and their chemical and reactivity properties have been well-established through intensive mechanistic studies of C−H bond activation reactions of alkanes occurring via H atom abstraction (Scheme 1A), C−H bond activation or epoxidation reactions of olefins (Scheme 1B,C), and oxidation reactions of sulfides (Scheme 1C).[11−16]

High-valent ruthenium−oxo complexes of heme and nonheme ligands have also been invoked as active oxidants in catalytic oxidation reactions.[17−19] In heme models, Ru−oxo porphyrin (Por) species have been shown to perform C−H bond activation of alkanes, most likely by $(Por)Ru^{V}O$ species, which are the Ru analogues of the cytochrome P450 Compound I species.[20−23] Oxidation reactions of alkanes and olefins by nonheme Ru complexes, wherein certain organic products are formed selectively in high yields, have long been known as well.[24−47] Such reactions are known to occur via H atom abstraction, hydride transfer, electron transfer, proton-coupled electron transfer (PCET), or oxygen atom transfer (OAT) mechanisms. For instance, oxidation of cumene by *cis*-$[Ru^{IV}(bpy)_2(py)(O)]^{2+}$ (bpy = 2,2′-bipyridine, py = pyridine) was first investigated several decades ago.[25] It was initially thought to occur through a hydride transfer mechanism[25] but was later shown to occur through a H atom abstraction mechanism.[35] One of the suggested pathways included the reaction of a cumyl radical with a second $Ru^{IV}O$ species (Scheme 1A, pathways *a*, *e*, and *f*). As multiple organic products were seen in this reaction as well as Ru^{II} products, it was concluded that this pathway acts parallel to oxygen rebound and desaturation-type reactions done by $Ru^{III}OH$ (Scheme 1A, pathways *b*, *d*, and *e*), followed by more downstream reactions in the pathway to the final products. A second example, also

Received: May 8, 2015
Published: June 15, 2015

DOI: 10.1021/jacs.5b04787
J. Am. Chem. Soc. 2015, 137, 8623−8632

Scheme 1. Proposed Mechanisms in Alkane Hydroxylation, Cyclohexene Oxidation, and Oxygen Atom Transfer Reactions by Metal−Oxo Species

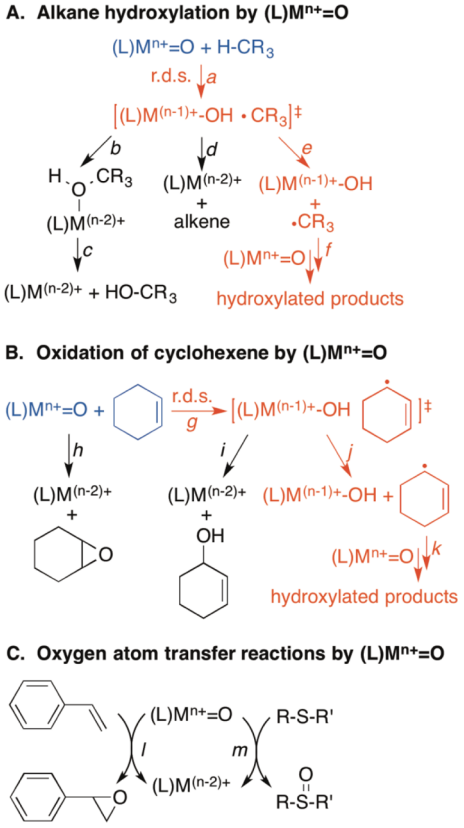

using cumene as a substrate but with different catalyst ligands, resulted in the experimental observation of $Ru^{III}OH$ and Ru^{III}−alkoxo species, described as intermediates of a rebound process (Scheme 1A, pathways *a*, *b*, and *c*).[45] A third example is the oxidation of cyclohexene and indene, which was likewise shown to occur through an initial C−H bond activation pathway rather than an epoxidation pathway (Scheme 1B, pathway *g* vs *h*).[32] The reactions were proposed to occur through many pathways that ultimately accounted for the formation of different organic products, kinetics, and spectra related to the reactions. Other substrates were also used in the mechanistic studies of $Ru^{IV}O$ complexes.[30,33−37]

Although efforts have been made to elucidate the mechanism(s) of C−H bond activation of benzylic and allylic C−H bonds by $Ru^{IV}O$ species,[24,28,29,31,32,34,35] theoretical studies have been underused in deciphering the distinct mechanistic steps of bond activation by $Ru^{IV}O$. While there have been some pure theoretical works in Ru−oxo chemistry (e.g., using (Por)$Ru^{V}O$ species),[22,23] combined experimental and theoretical studies give a much deeper insight into the reaction mechanisms, as shown by our earlier work on the fundamental differences between two-state and single-state reactivity patterns of $Fe^{IV}O$ and $Ru^{IV}O$ complexes in C−H bond activation reactions.[48] Furthermore, combining experimental and theoretical methods has enabled us to establish that the mechanism of C−H bond activation of hydrocarbons by metal−oxo species in nonheme synthetic model reactions is different from the oxygen rebound mechanism that has been well-established for heme enzymes and their models. In the oxygen rebound mechanism, H atom abstraction results in the formation of a carbon radical and a metal−hydroxo complex (Scheme 1A, pathway *a*), and this is followed by a rebound to the carbon radical from the metal−hydroxo complex which produces alcohol or by a desaturation process (Scheme 1A, pathways *b*, *c*, and *d*).[49−53] However, in the case of a dissociative oxygen non-rebound reaction, the substrate radical escapes from the cage and then reacts with a second metal−oxo molecule to give hydroxylated products (Scheme 1A, pathways *e* and *f*, for alkane hydroxylation; Scheme 1B, pathways *j* and *k*, for allylic C−H bond activation).[54−59] We have recently shown that this radical dissociative mechanism prevails in C−H bond activation reactions by $Fe^{IV}O$, $Mn^{IV}O$, $Cr^{IV}O$, and $Fe^{V}O$ catalysts in nonheme systems.[54−59] Very recently, we have also shown that an interplay of tunneling and spin inversion probability has to be taken into account in modeling this kind of C−H activation reaction.[59]

Herein we provide results obtained from combined experimental and theoretical studies that strongly support that the C−H bond activation of alkanes by a mononuclear nonheme $Ru^{IV}O$ complex, $[Ru^{IV}(O)(terpy)(bpm)]^{2+}$ (**1**) (terpy = 2,2′:6′,2″-terpyridine, bpm = 2,2′-bipyrimidine), whose density functional theory (DFT)-optimized structure is shown in Figure 1, follows a dissociative oxygen non-rebound mechanism (Scheme 1A, reaction pathway *e*). While the oxidation of styrene and thioanisole by **1** occurs via an OAT mechanism, we show that the oxidation of cyclohexene by **1** affords products resulting from a C−H bond activation reaction rather than an epoxidation reaction. All of the results obtained experimentally in this study have been replicated in silico by theoretical calculations, detailing the precise steps involved in the oxidation reactions.

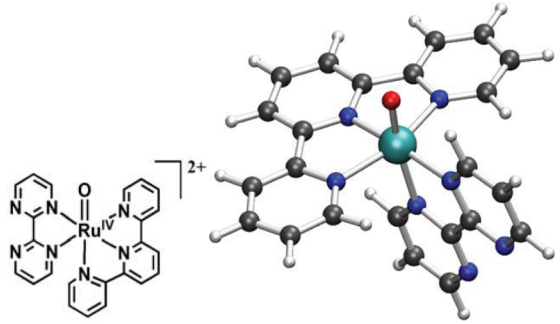

Figure 1. (left) Chemical structure of complex **1**. (right) Structure of **1** optimized by DFT at the B3LYP/LACVP level. Atom colors: aqua = Ru, red = O, blue = N, black = C, white = H.

RESULTS AND DISCUSSION

Generation and Characterization of 1. The ruthenium(IV)−oxo complex **1** was synthesized by reacting $[Ru^{II}(terpy)(bpm)(H_2O)](ClO_4)_2$ with PhIO in CH_3CN at 25 °C.[60] Upon the addition of PhIO (1.2 equiv, dissolved in MeOH) to a solution containing the starting Ru^{II} complex, the UV−vis band at 485 nm decayed within 2 min with the concurrent appearance of a new peak at 445 nm (ε = 2000 M^{-1} cm^{-1}) (Figure 2a). The yellowish-orange species **1**, which was metastable at 25 °C ($t_{1/2}$ ∼ 1 h), was characterized by various spectroscopic methods. Electrospray ionization mass spectrometry (ESI-MS) spectrum of **1** exhibited prominent mass peaks at m/z = 254.6 and 608.0, whose mass and isotope distribution patterns correspond to $[Ru^{IV}(O)(terpy)(bpm)]^{2+}$ (calcd m/z =

DOI: 10.1021/jacs.5b04787
J. Am. Chem. Soc. 2015, 137, 8623−8632

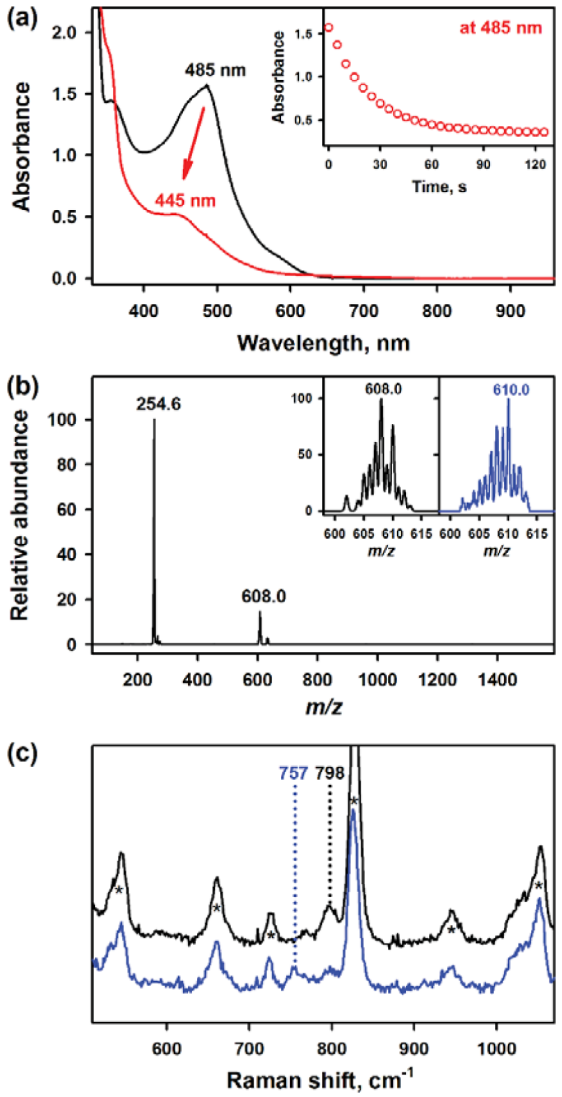

Figure 2. (a) UV−vis spectra of $[Ru(terpy)(bpm)(H_2O)]^{2+}$ (0.25 mM, black line) and **1** (0.25 mM, red line) in CH_3CN at 25 °C. The inset shows the time course of the decay of $[Ru(terpy)(bpm)(H_2O)]^{2+}$ monitored at 485 nm. (b) ESI-MS spectrum of **1**. Peaks at m/z = 254.6 and 608.0 correspond to $[Ru^{IV}(O)(terpy)(bpm)]^{2+}$ (calcd m/z = 254.5) and $[Ru^{IV}(O)(terpy)(bpm)(ClO_4)]^{+}$ (calcd m/z = 608.0), respectively. The insets show the observed isotope distribution patterns for **1**-^{16}O at m/z = 608.0 (left panel) and **1**-^{18}O at m/z = 610.0 (right panel). (c) Resonance Raman spectra of **1**-^{16}O (black line) and **1**-^{18}O (blue line) in CH_3CN recorded with 406.7 nm excitation at −20 °C. The peaks marked asterisks (*) are from the solvent.

254.5) and $[Ru^{IV}(O)(terpy)(bpm)(ClO_4)]^{+}$ (calcd m/z = 608.0), respectively (Figure 2b). When **1** was generated with isotopically labeled PhI^{18}O, the mass peak at m/z = 608.0 due to **1**-^{16}O shifted to m/z = 610.0 due to **1**-^{18}O, indicating that **1** contains one oxygen atom. The resonance Raman spectrum of **1** exhibited a vibration at 798 cm^{-1}, which shifted to 757 cm^{-1} upon introduction of ^{18}O (Figure 2c). The observed isotopic shift of $\Delta\nu$ = 41 cm^{-1} upon ^{18}O substitution is in good agreement with the calculated value of $\Delta\nu$ = 41 cm^{-1} for the Ru−O diatomic vibration, as reported for other Ru(IV)−oxo species.[19,43,45] It is also in agreement with our DFT-calculated Ru−O vibrational frequency, which was found to be 796 cm^{-1} and shifted to 758 cm^{-1} upon ^{18}O substitution. The X-band electron paramagnetic resonance (EPR) spectrum of **1** was silent, consistent with **1** being an integer spin system. The spin state of **1** was then determined using the ^{1}H NMR technique of Evans[61,62] (see the Experimental Section); the magnetic moment of 3.3 μ_B at −20 °C indicates that **1** is an intermediate-spin (S = 1) $Ru^{IV}(O)$ complex (see Figure S1 in the Supporting Information (SI) for the ^{1}H NMR spectrum of **1**). DFT calculations confirmed that the lowest spin state was the S = 1 state, whose Gibbs free energy was 14.1 and 60.3 kcal mol^{-1} lower than those of the S = 0 and S = 2 states, respectively (Table S1 in the SI). The high energy of the S = 2 state is due to high-lying σ^*_{xy} and $\sigma^*_{z^2}$ orbitals, effectively ruling out any reactions associated with participation of these orbitals. Taken together, the spectroscopic and computational data clearly demonstrate that **1** is an S = 1 $[Ru^{IV}(O)(terpy)(bpm)]^{2+}$ complex (Figure 1).

C−H Bond Activation by 1. We carried out the C−H bond activation reactions using substrates with bond dissociation energies (BDEs) between 81.0 kcal mol^{-1} (triphenylmethane) and 95.5 kcal mol^{-1} (cyclooctane) in CH_3CN at 25 °C. Upon addition of ethylbenzene to a solution of **1**, the UV−vis peak at 445 nm was slowly converted to a new peak at 460 nm with clean isosbestic points at 337, 363, and 628 nm (Figure 3a). The first-order rate constants (k_{obs}), determined by pseudo-first-order fitting of the kinetic data for the formation of the new peak at 460 nm, increased proportionally with increasing ethylbenzene concentration (Figure 3b), leading us to determine a second-order rate constant (k_2) of 5.0 × 10^{-1} M^{-1} s^{-1}. Similarly, when we used deuterated ethylbenzene-d_{10} as a substrate, the value of k_2 = 2.3 × 10^{-2} M^{-1} s^{-1} was obtained (Figure 3b). Thus, a kinetic isotope effect (KIE) value of 22(2) was obtained in the oxidation of ethylbenzene versus ethylbenzene-d_{10} in CH_3CN at 25 °C. Second-order rate constants for other alkanes were determined similarly (Figure S2 in the SI), and Figure 3c shows a good linear correlation between the logarithm of k_2' and the C−H BDE of the substrate. On the basis of the large KIE value and the good correlation between log(k_2') and the substrate BDE, we conclude that the C−H bond activation of alkanes by **1** occurs via H atom abstraction from substrate C−H bonds as the rate-determining step (r.d.s.) (Scheme 1A, pathway *a*).[32,35]

Product analysis of the reaction solution of **1** and ethylbenzene revealed the formation of 1-phenylethanol (27(4)%), acetophenone (8(3)%), and styrene (2(1)%) under an Ar atmosphere. The total product yield of 45%, calculated accounting for the fact that acetophenone is a four-electron oxidation product, suggests that one molecule of substrate was oxidized by two molecules of $Ru^{IV}O$ (vide infra). When the ethylbenzene oxidation was performed using **1**-^{18}O, the 1-phenylethanol product was found to contain 71(5)% ^{18}O (Figure S3 in the SI), demonstrating that the source of oxygen in the 1-phenylethanol product was **1**-^{18}O. When the reaction was carried out in the presence of air, the yields of 1-phenylethanol, acetophenone, and styrene were 16(4), 30(3), and 8(3)%, respectively. In addition, when the oxidation of ethylbenzene by **1** was performed in the presence of CCl_3Br (500 equiv) under an Ar atmosphere, (1-bromoethyl)benzene was obtained as the sole product.[54]

We also characterized the Ru product formed in the reaction of **1** and ethylbenzene by electron paramagnetic resonance (EPR) spectroscopy and ESI-MS. The X-band EPR spectrum of the Ru product showed signals with g = 2.42, g = 2.16, and g = 1.91 (Figure S4a in the SI), indicating the oxidation state of

DOI: 10.1021/jacs.5b04787
J. Am. Chem. Soc. 2015, 137, 8623−8632

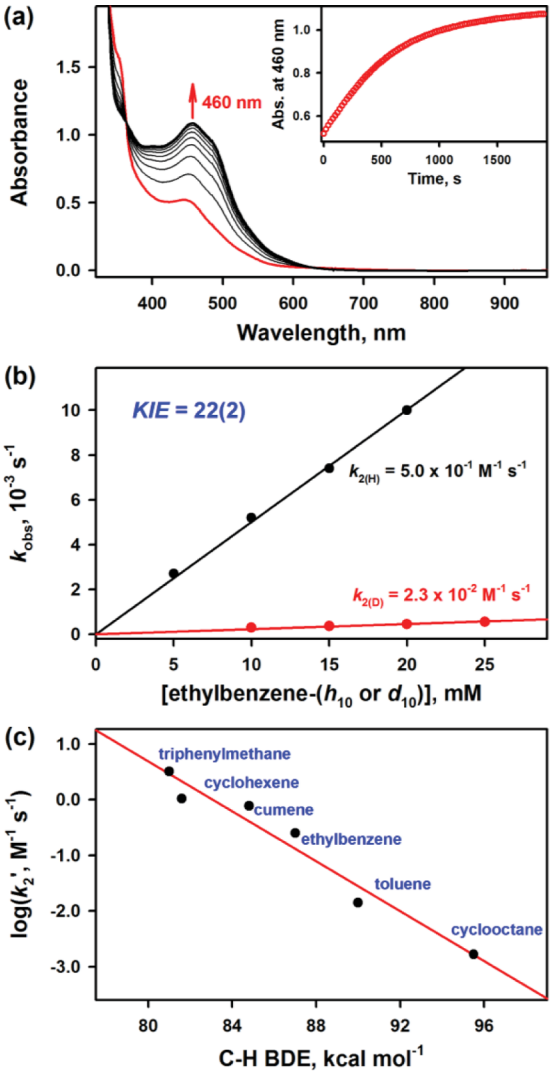

Figure 3. (a) UV−vis spectral changes observed in the reaction of **1** (0.25 mM, red line) and ethylbenzene (5.0 mM) in CH_3CN at 25 °C. The inset shows the time course of the reaction monitored at 460 nm. (b) Plots of the pseudo-first-order rate constants k_{obs} (in s^{-1}) against the concentrations of ethylbenzene-h_{10} (black circles) and ethylbenzene-d_{10} (red circles) to determine the second-order rate constants k_2 in CH_3CN at 25 °C. (c) Plot of log k_2' versus the substrate C−H BDE. The k_2' values were obtained by dividing the second-order rate constants (k_2) by the numbers of equivalent target C−H bonds in the substrates.

+3 for the Ru product.[45] The ESI-MS spectrum of the solution exhibited a prominent mass peak at m/z = 255.1, whose mass and isotope distribution pattern correspond to $[Ru^{III}(terpy)(bpm)(OH)]^+$ (calcd m/z = 255.0) (Figure S4b in the SI). Furthermore, addition of 1 equiv of 1,1′-dimethylferrocene (Me_2Fc) to the solution after completion of the reaction of **1** and ethylbenzene resulted in the formation of Ru^{II} and 1,1′-dimethylferrocenium ion (Me_2Fc^+) in >90% yield (Figure S5a in the SI), indicating that the Ru^{III} species produced was reduced to Ru^{II} by Me_2Fc (also see Figure S5b in the SI for the ESI-MS spectrum). Thus, all of the results discussed above strongly support that a $Ru^{III}OH$ species, not a Ru^{II} species, was formed in the reaction of ethylbenzene with **1**.

The observations described above are contrary to the oxygen rebound mechanism, since the hydroxylation of alkanes by $Ru^{IV}O$ species should yield Ru^{II} species as a two-electron-reduced product in the oxygen rebound mechanism.[34,35,45] Since we could not rule out the possibility that the formation of Ru^{III} resulted from comproportionation of $Ru^{IV}(O)$ and Ru^{II} species, we carried out a control experiment in which equal amounts of **1** and $[Ru^{II}(terpy)(bpm)]^{2+}$ were reacted. In this reaction, no formation of Ru^{III} species was observed by UV−vis, EPR, and ESI-MS analyses (Figure S6 in the SI), leading us to conclude that the $Ru^{III}OH$ species was formed exclusively from the H atom abstraction reaction of the alkane by **1** and not from comproportionation of $Ru^{IV}(O)$ and Ru^{II} species.

In view of this, how is the $Ru^{III}OH$ species formed in the C−H bond activation of alkanes by **1**? We propose that after the $Ru^{III}OH$ and alkyl radical species are formed in the first step of the C−H bond activation by **1** (Scheme 1A, pathway *a*), the preferred pathway is the dissociation process (Scheme 1A, pathway *e*) rather than the oxygen rebound (Scheme 1A, pathways *b* and *c*) and desaturation (Scheme 1A, pathway *d*) processes. This conclusion is based on the results of the organic products formed in the presence of O_2 (i.e., via dissociation of the substrate radical from $Ru^{III}OH$ and reaction with O_2 to give hydroxylated products) and in the presence of CCl_3Br (i.e., via dissociation of the substrate radical from $Ru^{III}OH$ and reaction with CCl_3Br to give brominated products) as well as the presence of the Ru^{III} product. These results are in line with our earlier observations reported for the reactions of nonheme $Fe^{IV}O$, $Mn^{IV}O$, $Cr^{IV}O$, and $Fe^{V}O$ complexes.[54−59]

To support the dissociation hypothesis, we performed DFT calculations on the reaction of **1** and ethylbenzene (Tables S2, S7, and S12 in the SI). The DFT calculations resulted in a reaction free energy barrier of 15.3 kcal mol^{-1} for the S = 1 state (^{3}**TS**$_E$ in Figure 4; the left superscript refers to the multiplicity $M = 2S + 1$ per convention) relative to the sum of the energies of the separated reactants (^{3}**R**$_{E+RuO}$, as opposed to the reactant complex, ^{3}**RC**$_E$). This step was found to be the r.d.s. (Scheme 1A, pathway *a*), with a barrier comparable to the experimental barrier of 18.3 kcal mol^{-1} determined from k_2' through the Eyring equation. A two-spin-state reaction was ruled out in this step of the reaction because the S = 0 state ^{1}**TS**$_E$ is high in energy (22.5 kcal mol^{-1}). Hence, after the initial H atom transfer (HAT) step, the resulting $Ru^{III}OH$ species is in the $S = {}^1/_2$ state, while the substrate has an α-radical, in total making it an S = 1 state (^{3}**I**$_E$). In the second step, the reaction has four pathway choices; (*i*) the rebound reaction (Scheme 1A, pathways *b* and *c*); (*ii*) abstraction of another H atom from the substrate to perform a desaturation reaction (Scheme 1A, pathway *d*); (*iii*) dissociation (Scheme 1A, pathway *e*); or (*iv*) changing the α-spin of the substrate to a β-spin and performing the rebound/desaturation/dissociation reaction on the potential surface of the S = 0 spin state. Choices (*i*) and (*ii*) are ruled out because their transition states, ^{3}**TS**$_{E\text{-}reb}$ and ^{3}**TS**$_{E\text{-}des}$, were found to be 28.4 and 27.8 kcal mol^{-1} above the reactants, respectively. The dissociation option (*iii*) is then much more preferable, with an exothermic dissociation free energy of 1.3 kcal mol^{-1} (i.e., the dissociated products ^{3}**P**$_{E^\bullet+RuOH}$ are 0.19 kcal mol^{-1} above ^{3}**R**$_{E+RuO}$).

Option (*iv*), the spin flip to reach ^{1}**I**$_E$, is possible in principle. As the S = 0 rebound (^{1}**TS**$_{E\text{-}reb}$) and desaturation (^{1}**TS**$_{E\text{-}des}$) transition states are very low (3.1 and 4.2 kcal mol^{-1}, respectively) and the spin−orbit coupling in Ru is large, this pathway would seem to be competitive with the S = 1 dissociation reaction. However, a spontaneous spin flip of a carbon-centered radical is not necessarily an ultrafast process.

DOI: 10.1021/jacs.5b04787
J. Am. Chem. Soc. 2015, 137, 8623−8632

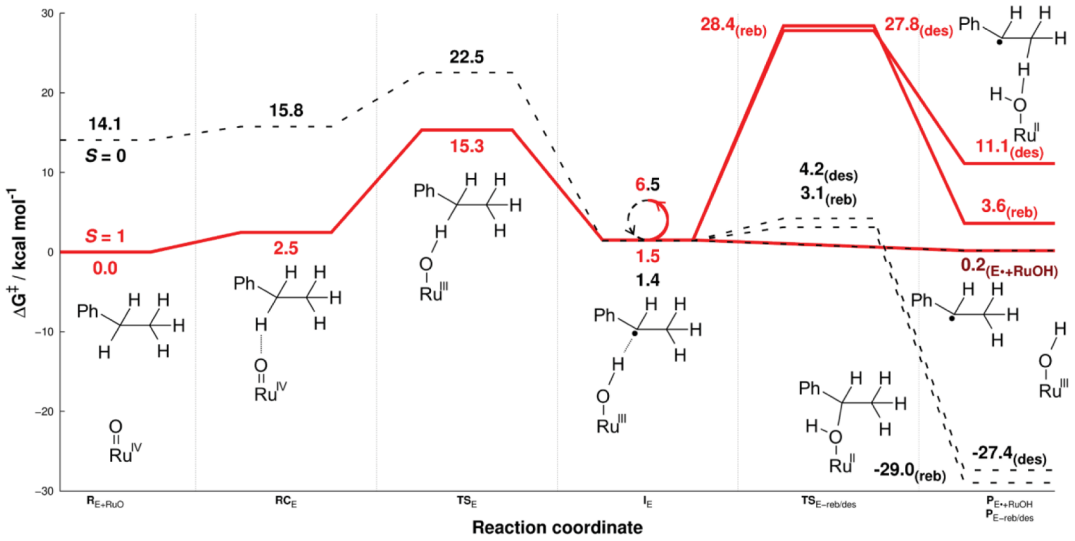

Figure 4. Reaction free energy profile for the ethylbenzene C–H activation reaction with **1** at 25 °C. The initial HAT reaction in the S = 1 state creates a substrate intermediate $^3\mathbf{I}_E$, which can react in a number of ways (see the text), including spin flipping (marked with a loop in the center of the graph) with an estimated minimum energy barrier of 5.0 kcal mol^{-1}. The lowest-energy pathway is therefore the S = 1 dissociation pathway, in which the product state ($^3\mathbf{P}_{E^{\bullet}+RuOH}$) is only 0.19 kcal mol^{-1} above the separated reactants, $^3\mathbf{R}_{E+RuO}$.

We have previously argued that even if we assume an ultrafast spin-flip process of 10^9 s^{-1}, this would still be equivalent to having an energy barrier of 5.0 kcal mol^{-1} according to the Eyring equation at room temperature.[56] This would not be competitive with the dissociation energy of 1.3 kcal mol^{-1}. Even if the spin flip occurs, however, the dissociation energy in the S = 0 state is still exothermic by 1.2 kcal mol^{-1}. Hence, the dissociation mechanism will likely be preferred anyhow, which is more in line with our experimental results showing 45% yield of products, compared to the projected 50% product yield in the dissociation mechanism.[54−59]

An additional issue in this reaction is tunneling, as indicated by the high experimental KIE. Using Eckart tunneling,[63] we found that the tunneling effect corresponds to lowering the S = 1 ethylbenzene-h_{10} and -d_{10} barriers by 1.8 and 1.0 kcal mol^{-1}, respectively (Table S2 in the SI). Without these effects, the KIE value would have been 7 using the free energies. With tunneling, the KIE value is 25, which is close to the experimental value of 22(2).

Epoxidation of Styrene by 1. We investigated olefin oxidation using styrene-h_8 and styrene-d_8 as substrates. Upon addition of styrene to a solution of **1** in CH_3CN at 25 °C, **1** decayed with the formation of a new peak at 450 nm (Figure 5a). The first-order rate constants (k_{obs}), determined by pseudo-first-order fitting of the kinetic data at 450 nm, increased proportionally with increasing substrate concentration, affording second-order rate constants of 1.6 × 10^{-1} M^{-1} s^{-1} for the reactions of both styrene-h_8 and styrene-d_8 (Figure 5b). The KIE value of 1 suggests that the reaction of **1** with the olefin does not occur via the H atom abstraction pathway but rather via OAT to the C=C double bond (Scheme 1C). Indeed, styrene oxide was formed as the major product (84(5)% yield), with the formation of a small amount of 2-phenylacetaldehyde (4(1)%) under an Ar atmosphere. In the reaction where **1**-^{18}O was used, the styrene oxide product contained 78(4)% ^{18}O (Figure S9 in the SI), suggesting that the oxygen in the styrene oxide product derived from the Ru^{IV}O species. EPR and ESI-MS characterization of the Ru product formed in the epoxidation reaction was also carried out. The

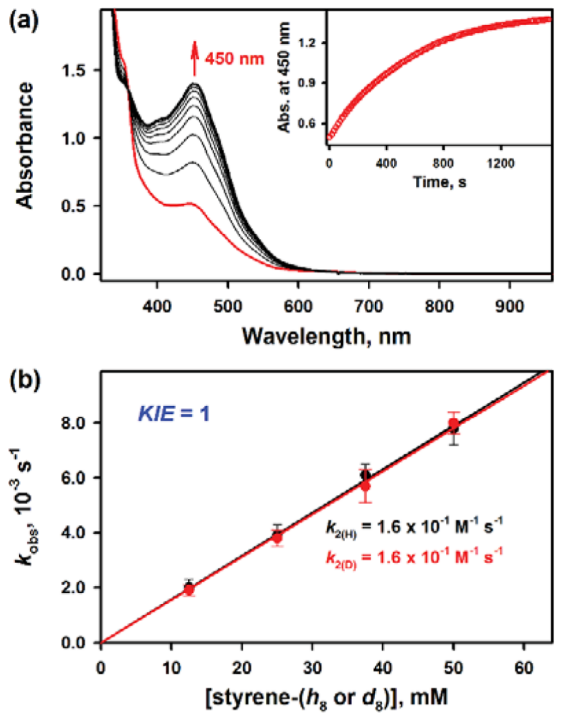

Figure 5. (a) UV–vis spectral changes observed in the reaction of **1** (0.25 mM, red line) and styrene (13 mM) in CH_3CN at 25 °C. The inset shows the time course of the reaction monitored at 450 nm. (b) Plots of pseudo-first-order rate constants k_{obs} (in s^{-1}) against the concentrations of styrene-h_8 (black circles) and styrene-d_8 (red circles) to determine the second-order rate constants k_2 and the KIE value in CH_3CN at 25 °C.

EPR spectrum was silent, suggesting the formation of Ru^{II} species as the end product. The ESI-MS data exhibited mass peaks corresponding to [Ru^{II}(terpy)(bpm)(CH_3CN)]$^{2+}$ (Figure S7 in the SI; also see Figure S8 in the SI for the conversion of the peak at 485 nm due to [Ru^{II}(terpy)(bpm)(H_2O)]$^{2+}$ to the peak at 450 nm due to [Ru^{II}(terpy)(bpm)(CH_3CN)]$^{2+}$). On the basis of the product analysis of the reaction solution of

DOI: 10.1021/jacs.5b04787
J. Am. Chem. Soc. 2015, 137, 8623−8632

1 and styrene, we conclude that styrene was oxidized to styrene oxide with the conversion of 1 to Ru^{II} species (Scheme 1C).

DFT calculations (Tables S3, S8, and S13 in the SI) reveal that in the $S = 1$ state this reaction is a two-step process (Figure 6). In the first step, 1 attacks the terminal C atom to form a

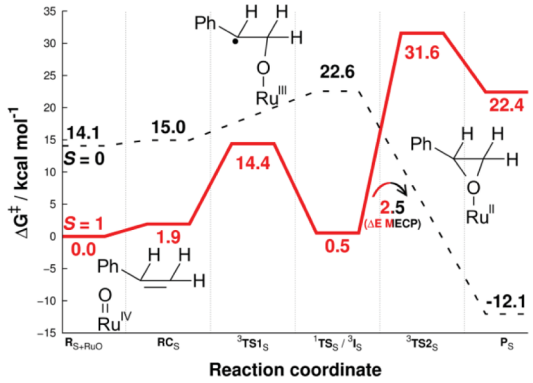

Figure 6. Reaction free energy profile for the epoxidation of styrene by 1 at 25 °C. The $S = 1$ surface features a two-step reaction mechanism, whereas the $S = 0$ surface shows a concerted one-step mechanism. A change in spin state (marked with an arrow) is proposed to occur after the ^3I_S step.

Ru−O−C-bonded intermediate ^3I_S via transition state $^3TS1_S$ at 14.4 kcal mol^{-1}. The alternative of attacking the other C atom in the ethane group has a higher transition state at 22.8 kcal mol^{-1} (not shown). The second step involves closing of the epoxide ring. However, it was found that this step goes over transition state $^3TS2_S$ at 31.6 kcal mol^{-1} to a Ru^{II} product that is at 22.4 kcal mol^{-1} (^3P_S). Hence, with the high barrier and an endothermic reaction free energy, the reaction at the $S = 1$ surface seems less probable.

In the $S = 0$ state, the epoxidation reaction features a one-step process over a single transition state ^1TS_S at 22.6 kcal mol^{-1}. This energy barrier is on the high side, especially compared with $^3TS1_S$ (14.4 kcal mol^{-1}) and also the experimental value (k_2 corresponding to 18.5 kcal mol^{-1}), but it is lower than $^3TS2_S$ (31.6 kcal mol^{-1}). Moreover, the Ru^{II} product ^1P_S is 34.5 kcal mol^{-1} more preferred than ^3P_s. It is a well-known experimental fact that Ru^{II} is an $S = 0$ species. Thus, it is clear that a spin flip to the $S = 0$ state has to occur somewhere along the reaction pathway. On the basis of our calculated data, we propose that this occurs at ^3I_S. In this way, the reaction can utilize the low $^3TS1_S$ to perform half of the reaction. Then the spin flip will allow the reaction to bypass the high $^3TS2_S$ and close the epoxide ring. Indeed, we found a minimum-energy crossing point (MECP) between these two states at 2.5 kcal mol^{-1} in electronic energy (ΔE), where optimization from this geometry with $S = 1$ led to ^3I_S and optimization with $S = 0$ led to ^1P_s. While we cannot calculate the final ΔG for the MECP (which would be dependent on, among other things, thermal contributions and spin inversion probabilities), if it is assumed that the corrections to the electronic energy are together less than 10 kcal mol^{-1}, the rate-limiting barrier is $^3TS1_S$.

C−H Bond Activation versus Epoxidation in the Oxidation of Cyclohexene by 1. We then investigated the reaction of 1 with cyclohexene-h_{10} and cyclohexene-d_{10} in CH_3CN at 25 °C. Upon addition of cyclohexene-h_{10} to the solution of 1, we observed the formation of a new peak at 460 nm (Figure S10 in the SI); the spectral changes were similar to those observed in the C−H bond activation of ethylbenzene by 1 (Figure 3a). The second-order rate constant $k_2 = 4.2(4)$ M^{-1} s^{-1} was determined, and a k_2' value was obtained by dividing k_2 by the number of equivalent target C−H bonds in cyclohexene (e.g., $k_2' = k_2/4$). The values of log k_2' for this reaction fit well into the line in Figure 3c, implying that the oxidation of cyclohexene by 1 occurs via a C−H bond activation process. When cyclohexene-d_{10} was used as a substrate, $k_2 = 1.1(1) \times 10^{-1}$ M^{-1} s^{-1} was obtained, thus giving a large KIE value of 38(3) (Figure 7).[32,34] Furthermore, the enthalpies and

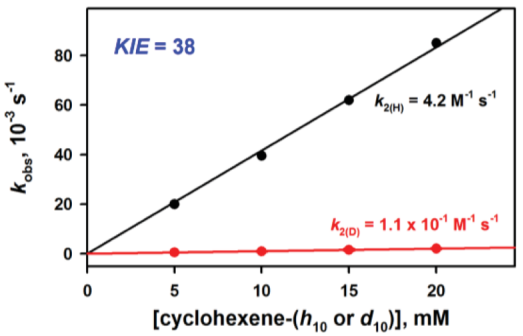

Figure 7. Plots of the pseudo-first-order rate constants k_{obs} (in s^{-1}) against the concentrations of cyclohexene-h_{10} (black circles) and cyclohexene-d_{10} (red circles) to determine the second-order rate constants k_2 and the KIE value in CH_3CN at 25 °C.

entropies of activation ($\Delta H^{\ddagger}$ and $\Delta S^{\ddagger}$, respectively) determined in the reactions of 1 with cyclohexene-h_{10} and cyclohexene-d_{10} were different depending on the substrate (Figure S11a in the SI), whereas the reactions of 1 with styrene-h_8 and styrene-d_8 showed that the $\Delta H^{\ddagger}$ and $\Delta S^{\ddagger}$ values were the same irrespective of the substrate (i.e., styrene and deuterated styrene) (Figure S11b in the SI). The results regarding the KIE and activation parameters indicate that the oxidation of cyclohexene by 1 occurs via a C−H bond activation reaction that includes tunneling. On the basis of the observed good correlation of the BDE with log k_2' (Figure 3c) and the large KIE value (Figure 7), we conclude that the H atom abstraction in the allylic α-C−H bond activation of cyclohexene by 1 is the r.d.s. (Scheme 1B, pathway *g*), which is different from the case of C=C double bond epoxidation of styrene (Scheme 1C).

When we carried out a product analysis of the oxidation of cyclohexene by 1 under an Ar atmosphere, a 26(3)% yield of cyclohex-2-enol and an 8(2)% yield of cyclohex-2-enone, corresponding to a total yield of 42% (26% + 2 × 8%), were obtained (Table 1). No formation of cyclohexene oxide

Table 1. Products of the Oxidation of Cyclohexene-h_{10} and Cyclohexene-d_{10} by 1[a]

substrate	product	yield (%)
cyclohexene-h_{10}	cyclohex-2-enol	26(3)
	cyclohex-2-enone	8(2)
	cyclohexene oxide	trace
cyclohexene-d_{10}	cyclohex-2-enol	21(2)
	cyclohex-2-enone	9(3)
	cyclohexene oxide	7(2)

[a]Reactions were run with 1 (1.0 mM) and substrate (50 mM) under an Ar atmosphere in CH_3CN at 25 °C. See the Experimental Section for product analysis.

DOI: 10.1021/jacs.5b04787
J. Am. Chem. Soc. 2015, 137, 8623−8632

product was observed in this reaction. Cyclohex-2-enol formed in the cyclohexene oxidation by **1**-^{18}O contained 82(4)% ^{18}O (Figure S12 in the SI), showing that the source of oxygen in the product was **1**. The decayed Ru product in the reaction of **1** and cyclohexene was determined to be a $Ru^{III}OH$ species by analysis of the reaction solution with ESI-MS and EPR spectroscopy and by carrying out a reaction with Me_2Fc; the Ru product was the same as that obtained in the oxidation of ethylbenzene by **1** (Figures S4–S6 in the SI). Interestingly, when we used cyclohexene-d_{10}, a small amount of cyclohexene oxide (7(2)% yield) was obtained along with cyclohex-2-enol (21(2)% yield) and cyclohex-2-enone (9(3)% yield).[59] Taken altogether, the experimental results demonstrate that H atom abstraction by **1** is the r.d.s. (Scheme 1B, pathway *g*) and that the reaction proceeds by the oxygen non-rebound mechanism (Scheme 1B, pathways *j* and *k*); the reaction mechanism is identical to that proposed for the oxidation of ethylbenzene by **1**.

DFT calculations (Tables S4, S9, and S14 in the SI) show that H atom abstraction of cyclohexene is the r.d.s., with ^{3}**TS**$_{C\text{-}HAT}$ at 14.6 kcal mol^{-1} (to be compared with the experimental value of 17.4 kcal mol^{-1} obtained from k_2') and ^{1}**TS**$_{C\text{-}HAT}$ at 21.5 kcal mol^{-1} (Figure 8). The oxygen non-rebound pathway is here indeed preferred as well, with free energies of −3.85, 28.0, and 24.8 kcal mol^{-1} for ^{3}**P**$_{C^{\bullet}+RuOH}$, ^{3}**TS**$_{C\text{-}reb}$, and ^{3}**TS**$_{C\text{-}des}$, respectively. Again, the S = 0 rebound and desaturation barriers are low, but the arguments against spin inversion in the case of ethylbenzene (vide supra) apply here as well. Likewise, the energetic profile for cyclohexene epoxidation is similar to that for styrene epoxidation described above. The S = 1 epoxidation occurs via a two-step process (with ^{3}**TS1**$_{C\text{-}OAT}$ and ^{3}**TS2**$_{C\text{-}OAT}$ equal to 19.1 and 33.0 kcal mol^{-1}, respectively), whereas the S = 0 surface contains one TS (^{1}**TS**$_{C\text{-}OAT}$ at 24.9 kcal mol^{-1}). Thus, spin inversion likely occurs here at ^{3}**I**$_{C\text{-}OAT}$ as well. However, since ^{3}**TS1**$_{C\text{-}OAT}$ (19.1 kcal mol^{-1}) is 4.5 kcal mol^{-1} higher than ^{3}**TS**$_{C\text{-}HAT}$ (14.6 kcal mol^{-1}), the H atom abstraction reaction takes precedence over the OAT reaction, in agreement with experiments. Upon deuteration, this difference is reduced to 2.6 kcal mol^{-1}, making partial epoxidation possible. The KIE value here is again more in agreement with the experimental value of 38 when tunneling effects are included (using Eckart tunneling, KIE = 24) than without tunneling (KIE = 6).

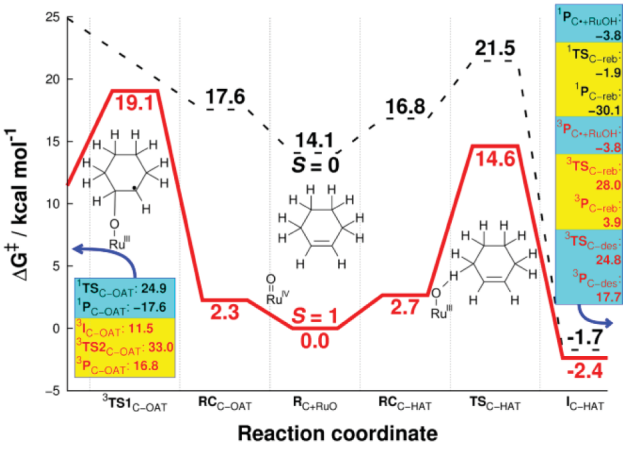

Figure 8. Epoxidation and C–H bond activation reaction free energy profiles for the oxidation of cyclohexene by **1** at 25 °C, showing only the first steps of the reactions. Starting from the middle of the graph, the C–H bond activation reaction goes to the right over a minimum barrier of 14.6 kcal mol^{-1}. Epoxidation, going to the left, has a higher minimum barrier of 19.1 kcal mol^{-1}. The entire shapes of the potential energy surfaces are similar to those for ethylbenzene for C–H bond activation (Figure 4) and styrene for epoxidation (Figure 6).

Sulfoxidation by 1. Finally, we investigated the oxidation of sulfides by **1**. Upon addition of thioanisole to a CH_3CN solution of **1** at −40 °C, the intermediate decayed along with the appearance of a peak at 485 nm (Figure S13 in the SI). The pseudo-first-order rate constant increased linearly with increasing thioanisole concentration, giving the second-order rate constant k_2 = 3.1(4) M^{-1} s^{-1} (Figure 9a). When *p*-X-substituted thioanisoles (X = OMe, Me, H, Br, and CN) were used in the sulfoxidation reaction, a ρ value of −2.1 was obtained from the Hammett plot of log k_2 against σ_p^+ (Figure 9b; Figure S14 in the SI shows the k_{obs} vs concentration plots to determine the k_2 values). This result indicates that the Ru–oxo group of **1** possesses an electrophilic character. In addition, when the rate constants were plotted against the oxidation potentials (E_{ox}) of the thioanisole derivatives, we observed a good linear correlation with a slope of −6.1 (Figure S15 in the SI), suggesting that the oxidation of thioanisoles by **1** occurs via a direct OAT mechanism (Scheme 1C, pathway *m*), as proposed in the oxidation of PPh_3 or PEt_3 by other $Ru^{IV}O$ species.[48,64]

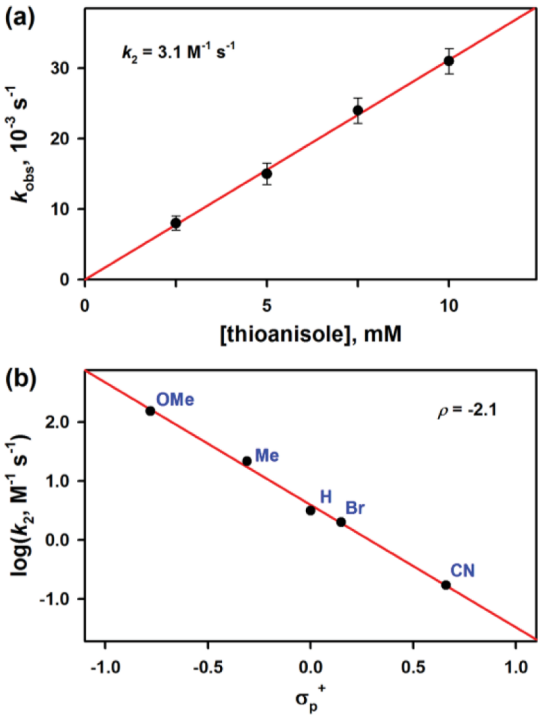

Figure 9. (a) Plot of the pseudo-first-order rate constant k_{obs} (in s^{-1}) against the thioanisole concentration to determine the second-order rate constant k_2 for the reaction of **1** and thioanisole in CH_3CN at −40 °C. (b) Hammett plot of log k_2 against σ_p^+ of *p*-X-substituted thioanisole derivatives (X = OMe, Me, H, Br, and CN).

Product analysis of the reaction solution revealed that methyl phenyl sulfoxide was formed as the sole product (85(5)% yield based on the amount of **1** used). When the thioanisole oxidation was performed using **1**-^{18}O, the methyl phenyl sulfoxide product contained 70(5)% ^{18}O, indicating that the

DOI: 10.1021/jacs.5b04787
J. Am. Chem. Soc. 2015, 137, 8623–8632

source of the oxygen atom in the sulfoxide product is **1** (Figure S16a in the SI). On the basis of the analysis of the reaction solution by EPR spectroscopy (not shown, but a silent EPR spectrum) and ESI-MS (Figure S16b in the SI), we found that a Ru^{II} species was formed as the decayed product of **1** in this reaction.

As shown in Figure 10, DFT calculations (Tables S5, S10, and S15 in the SI) show a single-step reaction with $^{3}TS_{T}$ at 18.7

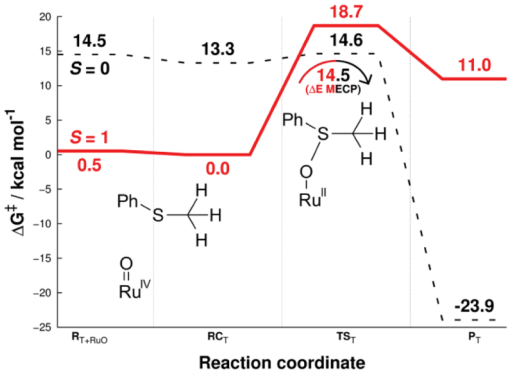

Figure 10. Reaction free energy profile for the sulfoxidation reaction of thioanisole by **1** at −40 °C. A spin-state change is predicted to occur near $^{1}TS_{T}$ so that the low-energy $^{1}TS_{T}$ can be utilized, which is consistent with the high experimental rates observed for this reaction.

kcal mol^{-1} at −40 °C. Interestingly, $^{1}TS_{T}$ is lower in energy at 14.6 kcal mol^{-1}, to which a contributing factor is the lower energy of the S = 0 Ru^{II} product. Given the very low experimentally determined energy barrier (13.0 kcal mol^{-1}), we propose that two-spin-state reactivity is in play here, where the reaction switches to the S = 0 surface to utilize the low-lying $^{1}TS_{T}$. In fact, an MECP was found just after $^{1}TS_{T}$ at ΔE = 14.5 kcal mol^{-1}, where geometry optimization on one side resulted in $^{3}RC_{T}$ and that on the other side resulted in $^{1}P_{T}$.

CONCLUSION

The C−H bond activation, epoxidation, and sulfoxidation reactions of mononuclear nonheme $Ru^{IV}O$ complexes have been investigated over the past three decades;[24−48] however, some of the proposed mechanisms in the oxidation reactions are still controversial and remain elusive, especially in the C−H bond activation reactions of alkanes and olefins containing allylic C−H bonds. Moreover, we have shown recently that mononuclear nonheme metal−oxo complexes conduct C−H bond activation reactions via an oxygen non-rebound mechanism rather than a conventional oxygen rebound mechanism.[54−59] We therefore reinvestigated the mechanisms of alkane hydroxylation, C−H bond activation versus olefin epoxidation in cyclohexene oxidation, and oxygen atom transfer reactions with a spectroscopically well-characterized $Ru^{IV}O$ complex, $[Ru^{IV}(O)(terpy)(bpm)]^{2+}$, using both experimental and theoretical methods. In the alkane hydroxylation, both the experimental and theoretical results demonstrate unambiguously that the dissociation of the substrate radical formed via a rate-determining H atom abstraction of an alkane C−H bond is more favorable than the oxygen rebound and desaturation processes. In the oxidation of olefins containing allylic C−H bonds, the experimental results show a preference for the H atom abstraction over the C=C double bond epoxidation in the oxidation of cyclohexene by **1**. This is further supported by DFT calculations, in which the free energy barrier for the C−H activation is indeed lower than that for epoxidation. In contrast, olefins without the allylic C−H bonds are oxidized to give epoxide products via an OAT mechanism. It has also been shown that in sulfoxidation reactions, **1** possesses an electrophilic character and conducts the sulfoxidation via an OAT mechanism. DFT calculations propose that two-spin-state reactivity is in play in both the epoxidation and sulfoxidation reactions. Overall, the present work adds one more piece of evidence that C−H bond activation of alkanes by mononuclear nonheme $Ru^{IV}O$ complexes occurs via an oxygen non-rebound mechanism, as we have shown in the reactions of mononuclear nonheme $Fe^{IV}O$, $Mn^{IV}O$, $Cr^{IV}O$, and $Fe^{V}O$ complexes.[54−58] We have also shown that C−H bond activation is a preferred pathway over C=C double bond epoxidation in the oxidation of cyclohexene by a mononuclear nonheme $Ru^{IV}O$ complex, similar to the case of a mononuclear nonheme $Fe^{IV}O$ complex.[59]

EXPERIMENTAL SECTION

Materials. $[Ru^{II}(terpy)(bpm)(H_2O)](ClO_4)_2$ and PhIO were prepared according to the literature procedures.[60,65−67] All other chemicals were obtained from Aldrich Chemical Co. and used without further purification, unless otherwise indicated. Solvents were dried according to reported procedures and distilled under Ar prior to use.[68] $H_2{}^{18}O$ (95% ^{18}O-enriched) was purchased from ICON Services Inc. (Summit, NJ, USA).

Instrumentation. UV−vis spectra were recorded on a Hewlett-Packard Agilent 8453 UV−vis spectrophotometer equipped with a circulating water bath or an UNISOKU cryostat system (USP-203, Japan). ESI-MS spectra were collected on an LCQ Advantage MAX quadrupole ion trap instrument (Thermo Finnigan, San Jose, CA, USA) by infusing samples directly into the source at 20 μL/min using a syringe pump. The spray voltage was set at 4.7 kV and the capillary temperature at 80 °C. EPR spectra were recorded at 5 K using an X-band Bruker EMX-plus spectrometer equipped with a dual-mode cavity (ER 4116DM). The low temperatures were achieved and controlled using an Oxford Instruments ESR900 liquid He quartz cryostat with an Oxford Instruments ITC503 temperature and gas flow controller. The experimental parameters for the EPR measurements were as follows: microwave frequency = 9.646 GHz, microwave power = 1.0 mW, modulation amplitude = 10 G, gain = 1×10^{4}, modulation frequency = 100 kHz, time constant = 40.96 ms, and conversion time = 85.00 ms. Resonance Raman spectra were recorded using a liquid-nitrogen-cooled CCD detector (model LN/CCD-1340 × 400PB, Princeton Instruments) attached to a 1 m single polychromator (model MC-100DG, Ritsu Oyo Kogaku). An excitation wavelength of 406.7 nm was provided by a Kr^{+} laser (Spectra Physics, BeamLok 2060-RM), with a power of 4.0 mW at the samples. All measurements were carried out with a spinning cell (1000 rpm) at −20 °C. Raman shifts were calibrated with indene, and the accuracy of the peak positions of the Raman bands was ±1 cm^{-1}. Product analysis was performed with an Agilent Technologies 6890N gas chromatograph (GC) and a FOCUS DSQ (dual-stage quadrupole) mass spectrometer (Thermo Finnigan, Austin, TX, USA) interfaced with a Finnigan FOCUS gas chromatograph (GC−MS). ^{1}H NMR spectra were measured with a Bruker model digital AVANCE III 400 FT-NMR spectrometer.

Generation and Characterization of 1. The yellowish-orange species **1** was generated by adding 1.2 equiv of PhIO (dissolved in MeOH) to a freshly prepared CH_3CN solution of $[Ru^{II}(terpy)(bpm)(H_2O)](ClO_4)_2$ (0.25 mM) at 25 °C. The ^{18}O-labeled $Ru^{IV}O$ complex (**1**-^{18}O) was prepared by using $PhI^{18}O$ in CH_3CN at 25 °C. $PhI^{18}O$ was prepared by mixing $PhI^{16}O$ (1.0 mM) solution with $H_2{}^{18}O$ (10 μL) and stirring for about 5 min. For the resonance Raman experiment, **1**-^{16}O and **1**-^{18}O were generated by adding 1.2 equiv of $PhI^{16}O$ and $PhI^{18}O$, respectively, to the solution of $[Ru^{II}(terpy)(bpm)(H_2O)](ClO_4)_2$ (4.0 mM) at 0 °C.

DOI: 10.1021/jacs.5b04787
J. Am. Chem. Soc. 2015, 137, 8623−8632

Spin-State Measurements by ^{1}H NMR Spectroscopy. The spin state of **1** was determined using the modified ^{1}H NMR method of Evans at −20 °C.[61,62] A WILMAD coaxial insert (sealed capillary) tube containing only the blank acetonitrile-d_3 solvent (with 1.0% tetramethylsilane (TMS)) was inserted into the normal NMR tube containing complex **1** (2.0 mM) dissolved in acetonitrile-d_3 (with 0.1% TMS). The chemical shift of the TMS peak in the presence of the paramagnetic metal complex was compared with that of the TMS peak in the inner NMR tube. The magnetic moment was calculated using the equation, $\mu = 0.0618(\Delta\nu T/2fM)^{1/2}$, where f is the oscillator frequency of the superconducting spectrometer (in MHz), T is the absolute temperature, M is the molar concentration of the metal ion, and ν is the difference between the frequencies of the two reference signals (in Hz).[62] The ^{1}H NMR Evans method allowed us to determine a magnetic moment of $3.3\mu_B$ for **1** in CH_3CN at −20 °C, indicating that **1** possesses an $S = 1$ spin state in CH_3CN solution.

Kinetic Measurements. All of the reactions were run in a 1 cm UV quartz cuvette and followed by monitoring the UV−vis spectral changes of the reaction solutions. Rate constants were determined under pseudo-first-order conditions (e.g., [substrate]/[**1**] > 10) by fitting the changes in absorbance for the formation of peaks at 460 nm in the C−H activation, 450 nm in styrene epoxidation, and 485 nm in thioanisole oxidation. Substrates with varying BDEs,[69] such as triphenylmethane (81.0 kcal mol^{-1}), cumene (84.5 kcal mol^{-1}), ethylbenzene (87.0 kcal mol^{-1}), toluene (90.0 kcal mol^{-1}), and cyclooctane (95.5 kcal mol^{-1}) were used in the C−H bond activation reactions with **1** in CH_3CN at 25 °C. The KIE value for the reaction of **1** and ethylbenzene was determined as the ratio of the k_2 values obtained in the C−H and C−D bond activation reactions of ethylbenzene-h_{10} and ethylbenzene-d_{10}, respectively. Similarly, the KIE values for the oxidation reactions of styrene and cyclohexene by **1** were obtained by using the ratios of k_2 values for styrene-h_8/styrene-d_8 and cyclohexene-h_{10}/cyclohexene-d_{10}, respectively. The reactions of **1** and thioanisoles were studied at −40 °C. The kinetic experiments were run at least in triplicate, and the reported data represent averages for these reactions. The values of k_2' were obtained by dividing the second-order rate constants k_2 by the number of equivalent target C−H bonds in the substrate.

Product Analysis. Products formed in the reactions of **1** with ethylbenzene, styrene, cyclohexene, and thioanisole were analyzed by GC and GC−MS, and the product yields were determined by comparing the peak areas of sample products against standard curves prepared with known authentic samples using decane as an internal standard. The oxidation of ethylbenzene was achieved by mixing 0.10 M ethylbenzene with 1.0 mM **1**. The ^{16}O and ^{18}O compositions in the oxygenated products of ethylbenzene, styrene, cyclohexene, and thioanisole were analyzed by comparing the relative abundances of m/z values that shifted by two mass units upon incorporation of ^{18}O from **1**-^{18}O with that of ^{16}O-products. The Ru products (Ru^{II} and Ru^{III} species) in the reaction solutions of **1** with substrates were analyzed using EPR spectroscopy and ESI-MS.

DFT Calculations. DFT[70] geometry optimizations and frequency calculations were done at the UB3LYP/LACVP level of theory[71−76] (except for the S atom, for which the 6-311G* basis set was employed) using the Gaussian 09 package.[77] The free energies were evaluated at 25 °C, except in the thioanisole sulfoxidation calculations, where they were evaluated at −40 °C, in line with experiments. Solvent effects (acetonitrile) were included in the geometry optimizations by means of the CPCM[78] as implemented in Gaussian 09. Single-point energy evaluations were done at the UB3LYP/Def2-TZVPP level[79] including the solvent. For singlet energies, as spin contamination was found to be severe in some cases, corrections were carried out by means of spin projection.[80] Dispersion effects were evaluated at the converged geometries by means of the DFT-D3 program using Becke−Johnson damping.[81] The energy reference point in each of the calculation series was the separated reactants (except for the sulfoxidation reaction), as this enabled us to obtain reasonable entropies (including dissociation entropy) in combination with reasonable dispersion values. These values were further corrected by a factor of 1.89 kcal mol^{-1}, as modeling of complexation in solvent requires a correct treatment of the standard state.[82] For the sulfoxidation reaction, the energy reference point was the reactant complex ^{3}**RC**$_T$, as this state was lower in free energy than the separated reactants. For the C−H activation reactions, tunneling corrections were earlier found to be essential,[83] and the barriers were therefore corrected using the unsymmetrical formalism of Eckart[63] as implemented in TheRate.[84] All of the energy values quoted in the text include all of the above-described effects (=ΔG), unless stated otherwise. MECPs were found using a shell script interface to Gaussian 09.[85] However, only the geometry and the electronic energy (ΔE) were evaluated at the MECP, as thermal contributions cannot be evaluated at nonstationary points with regard to one specific spin state. As the Def2-TZVPP energies were different for the different spin states at the LACVP-optimized structures at the MECP, the average was taken as the MECP Def2-TZVPP value.

■ ASSOCIATED CONTENT

Supporting Information

Figures S1−S16, Tables S1−S15, and DFT-calculated structure coordinates. The Supporting Information is available free of charge on the ACS Publications website at DOI: 10.1021/jacs.5b04787.

■ AUTHOR INFORMATION

Corresponding Author

*wwnam@ewha.ac.kr

Author Contributions

‖S.N.D. and K.-B.C. contributed equally.

Notes

The authors declare no competing financial interest.

■ ACKNOWLEDGMENTS

The authors acknowledge support from the the NRF of Korea through CRI (NRF-2012R1A3A2048842 to W.N.), MSIP (2013R1A1A2062737 to K.-B.C.), and GRL (NRF-2010-00353 to W.N.). S.S. acknowledges the Israel Science Foundation (ISF Grant 1183/12). S.N.D. thanks Goa University (Goa, India) for a grant of leave.

■ REFERENCES

(1) Ortiz de Montellano, P. R. *Cytochrome P450: Structure, Mechanism, and Biochemistry*, 3rd ed.; Springer: Berlin, 2005.
(2) Gunay, A.; Theopold, K. H. *Chem. Rev.* **2010**, *110*, 1060.
(3) Huynh, M. H. V.; Meyer, T. J. *Chem. Rev.* **2007**, *107*, 5004.
(4) Mayer, J. M. *Acc. Chem. Res.* **1998**, *31*, 441.
(5) Mayer, J. M. *Acc. Chem. Res.* **2011**, *44*, 36.
(6) Borovik, A. S. *Chem. Soc. Rev.* **2011**, *40*, 1870.
(7) Hohenberger, J.; Ray, K.; Meyer, K. *Nat. Commun.* **2012**, *3*, No. 720.
(8) Ray, K.; Heims, F.; Schwalbe, M.; Nam, W. *Curr. Opin. Chem. Biol.* **2015**, *25*, 159.
(9) Chen, Z.; Yin, G. *Chem. Soc. Rev.* **2015**, *44*, 1083.
(10) Fukuzumi, S. *Dalton Trans.* **2015**, *44*, 6696.
(11) Nam, W. *Acc. Chem. Res.* **2007**, *40*, 522.
(12) Shaik, S.; Hirao, H.; Kumar, D. *Acc. Chem. Res.* **2007**, *40*, 532.
(13) Green, M. T. *Curr. Opin. Chem. Biol.* **2009**, *13*, 84.
(14) De Visser, S. P.; Rohde, J.-U.; Lee, Y.-M.; Cho, J.; Nam, W. *Coord. Chem. Rev.* **2013**, *257*, 381.
(15) Nam, W.; Lee, Y.-M.; Fukuzumi, S. *Acc. Chem. Res.* **2014**, *47*, 1146.
(16) Ray, K.; Pfaff, F. F.; Wang, B.; Nam, W. *J. Am. Chem. Soc.* **2014**, *136*, 13942.
(17) Pagliaro, M.; Campestrini, S.; Ciriminna, R. *Chem. Soc. Rev.* **2005**, *34*, 837.
(18) Chan, S. L.-F.; Kan, Y.-H.; Yip, K.-L.; Huang, J.-S.; Che, C.-M. *Coord. Chem. Rev.* **2011**, *255*, 899.
(19) Ishizuka, T.; Ohzu, S.; Kojima, T. *Synlett* **2014**, *25*, 1667.

DOI: 10.1021/jacs.5b04787
J. Am. Chem. Soc. 2015, 137, 8623−8632

(20) Groves, J. T.; Quinn, R. *J. Am. Chem. Soc.* **1985**, *107*, 5790.
(21) Liu, C.-J.; Yu, W.-Y.; Li, S.-G.; Che, C.-M. *J. Org. Chem.* **1998**, *63*, 7364.
(22) Ogliaro, F.; de Visser, S. P.; Groves, J. T.; Shaik, S. *Angew. Chem., Int. Ed.* **2001**, *40*, 2874.
(23) Sharma, P. K.; de Visser, S. P.; Ogliaro, F.; Shaik, S. *J. Am. Chem. Soc.* **2003**, *125*, 2291.
(24) Thompson, M. S.; Meyer, T. J. *J. Am. Chem. Soc.* **1982**, *104*, 4106.
(25) Thompson, M. S.; Meyer, T. J. *J. Am. Chem. Soc.* **1982**, *104*, 5070.
(26) Takeuchi, K. J.; Thompson, M. S.; Pipes, D. W.; Meyer, T. J. *Inorg. Chem.* **1984**, *23*, 1845.
(27) Dobson, J. C.; Seok, W. K.; Meyer, T. J. *Inorg. Chem.* **1986**, *25*, 1514.
(28) Roecker, L.; Meyer, T. J. *J. Am. Chem. Soc.* **1987**, *109*, 746.
(29) Seok, W. K.; Meyer, T. J. *J. Am. Chem. Soc.* **1988**, *110*, 7358.
(30) Stultz, L. K.; Binstead, R. A.; Reynolds, M. S.; Meyer, T. J. *J. Am. Chem. Soc.* **1995**, *117*, 2520.
(31) Trammell, S. A.; Wimbish, J. C.; Odobel, F.; Gallagher, L. A.; Narula, P. M.; Meyer, T. J. *J. Am. Chem. Soc.* **1998**, *120*, 13248.
(32) Stultz, L. K.; Huynh, M. H. V; Binstead, R. A.; Curry, M.; Meyer, T. J. *J. Am. Chem. Soc.* **2000**, *122*, 5984.
(33) Meyer, T. J.; Huynh, M. H. V. *Inorg. Chem.* **2003**, *42*, 8140.
(34) Bryant, J. R.; Mayer, J. M. *J. Am. Chem. Soc.* **2003**, *125*, 10351.
(35) Bryant, J. R.; Matsuo, T.; Mayer, J. M. *Inorg. Chem.* **2004**, *43*, 1587.
(36) Matsuo, T.; Mayer, J. M. *Inorg. Chem.* **2005**, *44*, 2150.
(37) Che, C.-M.; Cheng, K.-W.; Chan, M. C. W.; Lau, T.-C.; Mak, C.-K. *J. Org. Chem.* **2000**, *65*, 7996.
(38) Che, C.-M.; Yu, W.-Y.; Chan, P.-M.; Cheng, W.-C.; Peng, S.-M.; Lau, K.-C.; Li, W.-K. *J. Am. Chem. Soc.* **2000**, *122*, 11380.
(39) Yip, W.-P.; Yu, W.-Y.; Zhu, N.; Che, C.-M. *J. Am. Chem. Soc.* **2005**, *127*, 14239.
(40) Yip, W.-P.; Ho, C.-M.; Zhu, N.; Lau, T.-C.; Che, C.-M. *Chem.—Asian J.* **2008**, *3*, 70.
(41) Lam, W. W. Y.; Man, W.-L.; Lau, T.-C. *Coord. Chem. Rev.* **2007**, *251*, 2238.
(42) Lam, W. W. Y.; Man, W.-L.; Leung, C.-F.; Wong, C.-Y.; Lau, T.-C. *J. Am. Chem. Soc.* **2007**, *129*, 13646.
(43) Hirai, Y.; Kojima, T.; Mizutani, Y.; Shiota, Y.; Yoshizawa, K.; Fukuzumi, S. *Angew. Chem., Int. Ed.* **2008**, *47*, 5772.
(44) Kojima, T.; Hirai, Y.; Ishizuka, T.; Shiota, Y.; Yoshizawa, K.; Ikemura, K.; Ogura, T.; Fukuzumi, S. *Angew. Chem., Int. Ed.* **2010**, *49*, 8449.
(45) Kojima, T.; Nakayama, K.; Ikemura, K.; Ogura, T.; Fukuzumi, S. *J. Am. Chem. Soc.* **2011**, *133*, 11692.
(46) Ohzu, S.; Ishizuka, T.; Hirai, Y.; Jiang, H.; Sakaguchi, M.; Ogura, T.; Fukuzumi, S.; Kojima, T. *Chem. Sci.* **2012**, *3*, 3421.
(47) Ishizuka, T.; Ohzu, S.; Kotani, H.; Shiota, Y.; Yoshizawa, K.; Kojima, T. *Chem. Sci.* **2014**, *5*, 1429.
(48) Dhuri, S. N.; Seo, M. S.; Lee, Y.-M.; Hirao, H.; Wang, Y.; Nam, W.; Shaik, S. *Angew. Chem., Int. Ed.* **2008**, *47*, 3356.
(49) Groves, J. T. *J. Chem. Educ.* **1985**, *62*, 928.
(50) Groves, J. T. *Proc. Natl. Acad. Sci. U.S.A.* **2003**, *100*, 3569.
(51) Groves, J. T. *J. Inorg. Biochem.* **2006**, *100*, 434.
(52) Shaik, S.; Kumar, D.; de Visser, S. P.; Altun, A.; Thiel, W. *Chem. Rev.* **2005**, *105*, 2279.
(53) Ortiz de Montellano, P. R. *Chem. Rev.* **2010**, *110*, 932.
(54) Cho, K.-B.; Wu, X.; Lee, Y.-M.; Kwon, Y. H.; Shaik, S.; Nam, W. *J. Am. Chem. Soc.* **2012**, *134*, 20222.
(55) Wu, X.; Seo, M. S.; Davis, K. M.; Lee, Y.-M.; Chen, J.; Cho, K.-B.; Pushkar, Y. N.; Nam, W. *J. Am. Chem. Soc.* **2011**, *133*, 20088.
(56) Cho, K.-B.; Shaik, S.; Nam, W. *J. Phys. Chem. Lett.* **2012**, *3*, 2851.
(57) Cho, K.-B.; Kang, H.; Woo, J.; Park, Y. J.; Seo, M. S.; Cho, J.; Nam, W. *Inorg. Chem.* **2014**, *53*, 645.
(58) Kwon, E.; Cho, K.-B.; Hong, S.; Nam, W. *Chem. Commun.* **2014**, *50*, 5572.
(59) Kwon, Y. H.; Mai, B. K.; Lee, Y.-M.; Dhuri, S. N.; Mandal, D.; Cho, K.-B.; Kim, Y.; Shaik, S.; Nam, W. *J. Phys. Chem. Lett.* **2015**, *6*, 1472.
(60) Concepcion, J. J.; Tsai, M.-K.; Muckerman, J. T.; Meyer, T. J. *J. Am. Chem. Soc.* **2010**, *132*, 1545.
(61) Evans, D. F. *J. Chem. Soc.* **1959**, 2003.
(62) Evans, D. F.; Jakubovic, D. A. *J. Chem. Soc., Dalton Trans.* **1988**, 2927.
(63) Eckart, C. *Phys. Rev.* **1930**, *35*, 1303.
(64) Moyer, B. A.; Sipe, B. K.; Meyer, T. J. *Inorg. Chem.* **1981**, *20*, 1475.
(65) Concepcion, J. J.; Jurss, J. W.; Templeton, J. L.; Meyer, T. J. *J. Am. Chem. Soc.* **2008**, *130*, 16462.
(66) Swavey, S.; Fang, Z.; Brewer, K. J. *Inorg. Chem.* **2002**, *41*, 2598.
(67) Saltzman, H.; Sharefkin, J. G. In *Organic Syntheses*; Wiley: New York, 1973; Collect. Vol. *V*.
(68) Armarego, W. L. F.; Chai, C. L. L. *Purification of Laboratory Chemicals*, 6th ed.; Pergamon Press: Oxford, U.K., 2009.
(69) Luo, Y.-R. *Handbook of Bond Dissociation Energies in Organic Compounds*; CRC Press: Boca Raton, FL, 2002.
(70) Kohn, W.; Sham, L. J. *Phys. Rev.* **1965**, *140*, A1133.
(71) Becke, A. D. *Phys. Rev. A* **1988**, *38*, 3098.
(72) Becke, A. D. *J. Chem. Phys.* **1993**, *98*, 1372.
(73) Becke, A. D. *J. Chem. Phys.* **1993**, *98*, 5648.
(74) Lee, C.; Yang, W.; Parr, R. G. *Phys. Rev. B* **1988**, *37*, 785.
(75) Hay, P. J.; Wadt, W. R. *J. Chem. Phys.* **1985**, *82*, 299.
(76) Francl, M. M.; Pietro, W. J.; Hehre, W. J.; Gordon, M. S.; DeFrees, D. J.; Pople, J. A. *J. Chem. Phys.* **1982**, *77*, 3654.
(77) Frisch, M. J.; Trucks, G. W.; Schlegel, H. B.; Scuseria, G. E.; Robb, M. A.; Cheeseman, J. R.; Scalmani, G.; Barone, V.; Mennucci, B.; Petersson, G. A.; Nakatsuji, H.; Caricato, M.; Li, X.; Hratchian, H. P.; Izmaylov, A. F.; Bloino, J.; Zheng, G.; Sonnenberg, J. L.; Hada, M.; Ehara, M.; Toyota, K.; Fukuda, R.; Hasegawa, J.; Ishida, M.; Nakajima, T.; Honda, Y.; Kitao, O.; Nakai, H.; Vreven, T.; Montgomery, J. A., Jr.; Peralta, J. E.; Ogliaro, F.; Bearpark, M.; Heyd, J. J.; Brothers, E.; Kudin, K. N.; Staroverov, V. N.; Kobayashi, R.; Normand, J.; Raghavachari, K.; Rendell, A.; Burant, J. C.; Iyengar, S. S.; Tomasi, J.; Cossi, M.; Rega, N.; Millam, J. M.; Klene, M.; Knox, J. E.; Cross, J. B.; Bakken, V.; Adamo, C.; Jaramillo, J.; Gomperts, R.; Stratmann, R. E.; Yazyev, O.; Austin, A. J.; Cammi, R.; Pomelli, C.; Ochterski, J. W.; Martin, R. L.; Morokuma, K.; Zakrzewski, V. G.; Voth, G. A.; Salvador, P.; Dannenberg, J. J.; Dapprich, S.; Daniels, A. D.; Farkas, Ö.; Foresman, J. B.; Ortiz, J. V.; Cioslowski, J.; Fox, D. J. *Gaussian 09*, revision D.01; Gaussian, Inc.: Wallingford, CT, 2009.
(78) Cossi, M.; Rega, N.; Scalmani, G.; Barone, V. *J. Comput. Chem.* **2003**, *24*, 669.
(79) Weigend, F.; Ahlrichs, R. *Phys. Chem. Chem. Phys.* **2005**, *7*, 3297.
(80) Yamaguchi, K.; Jensen, F.; Dorigo, A.; Houk, K. N. *Chem. Phys. Lett.* **1988**, *149*, 537.
(81) Grimme, S.; Ehrlich, S.; Goerigk, L. *J. Comput. Chem.* **2011**, *32*, 1456.
(82) Winget, P.; Cramer, C. J.; Truhlar, D. G. *Theor. Chem. Acc.* **2004**, *112*, 217.
(83) Mandal, D.; Ramanan, R.; Usharani, D.; Janardanan, D.; Wang, B.; Shaik, S. *J. Am. Chem. Soc.* **2015**, *137*, 722.
(84) Duncan, W. T.; Bell, R. L.; Truong, T. N. *J. Comput. Chem.* **1998**, *19*, 1039.
(85) Harvey, J. N.; Aschi, M.; Schwarz, H.; Koch, W. *Theor. Chem. Acc.* **1998**, *99*, 95.

DOI: 10.1021/jacs.5b04787
J. Am. Chem. Soc. 2015, 137, 8623−8632